SUPPORTING INFORMATION

Heme bioavailability and signaling in response to stress in yeast cells

David A. Hanna, Rebecca Hu, Hyojung Kim, Osiris Martinez-Guzman, Matthew P. Torres, and Amit R. Reddi

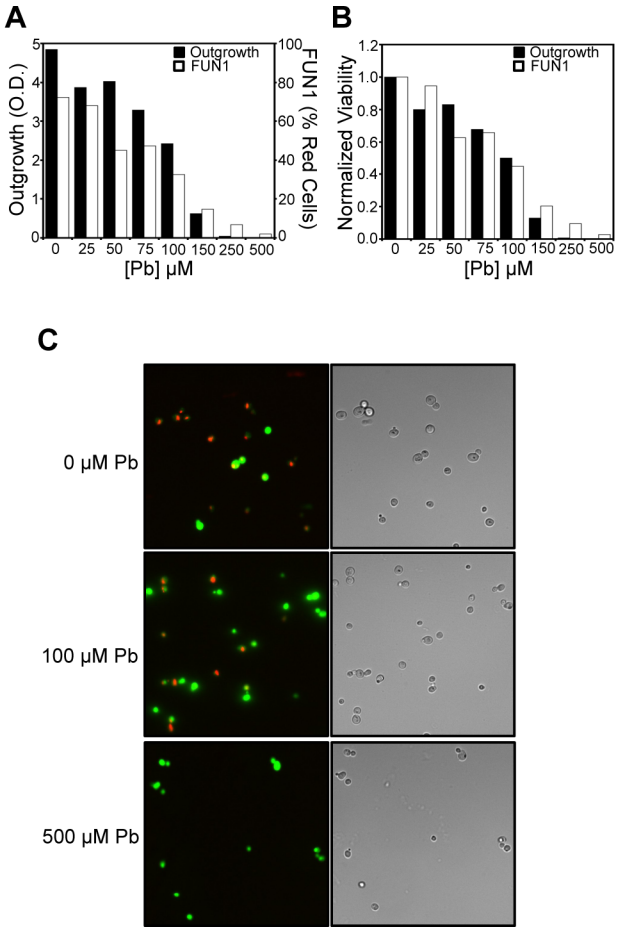

Fig. S1. Correlation between yeast cell viability as scored by outgrowth and a dye, FUN-1, that is sensitive to metabolic activity. (**A**) Outgrowth and FUN-1 measured viability was plotted as a function of [Pb] without normalization. Cell viability using FUN-1 was measured by taking the fraction of cells exhibiting red punctate fluorescence of the dye, which is indicative of metabolically active cells, and dividing over the total number of fluorescence positive cells that displayed either red punctate fluorescence or diffuse green fluorescence, which is indicative of metabolically inactive cells. (**B**) The data in **A** was normalized to the outgrowth or FUN-1 based viability at 0 µM [Pb]. These data are representative of two independent trials.

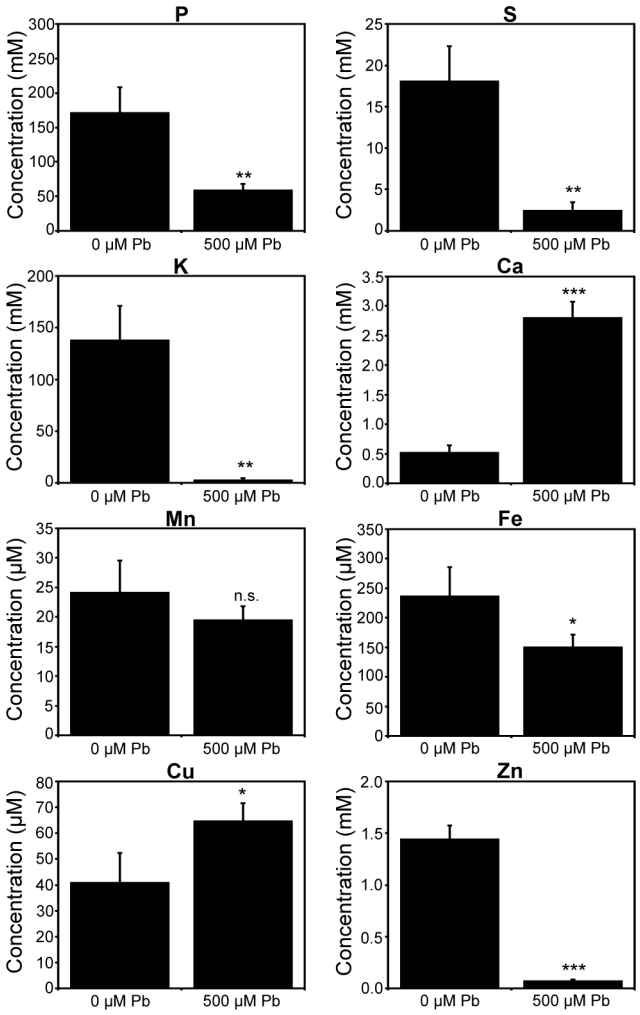

Fig. S2. Elemental analysis of Pb^{2+} treated cells from **Fig. 3.** All data represent the mean ± SD of triplicate cultures and statistical significance was assessed using a two-sample t-test. Black asterisks represent the statistical significance between the treated and untreated samples. * P < 0.05, ** P < 0.005, *** P < 0.0005, n.s. not significant.

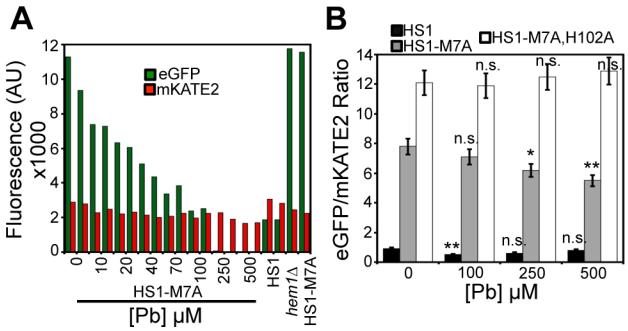

Fig. S3. The Pb^{2+}-dependent changes in heme sensor fluorescence ratios are not due to degradation of sensor and are heme dependent. (**A**) The eGFP (ex. 488 nm, em. 510 nm) and mKATE2 (ex. 588 nm, em. 620 nm) fluorescence channels that give rise to the HS1-M7A eGFP/mKATE2 ratios depicted in **Fig. S2A.** The relatively constant mKATE2 fluorescence emission across a wide array of Pb^{2+} doses indicates that sensor expression is stable. (**B**) A sensor variant that cannot bind heme, HS1-M7A, H102A, does not exhibit Pb^{2+}-dependent changes in eGFP/mKATE2 fluorescence ratio relative to the heme sensor, HS1-M7A. This suggests that the change in sensor fluorescence emission is due to heme and not Pb^{2+}-dependent, heme-independent changes in sensor fluorescence. All data represent the mean ± SD of triplicate cultures and statistical significance was assessed using a two-sample t-test. These data support **Fig. 4**. Black asterisks represent the statistical significance between the treated and untreated samples. * P ≤ 0.05, ** P < 0.01, n.s. not significant.

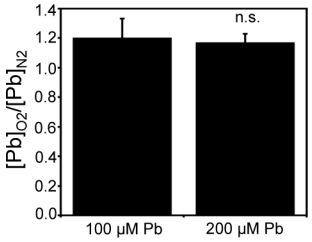

Fig. S4. Anaerobic and aerobic Pb^{2+} uptake are virtually identical. Intracellular Pb was measured by TXRF after treatment with a bolus of 100 µM or 200 µM $Pb(NO_3)_2$ that was administered either anaerobically (N_2) or aerobically (O_2) as described in the "Experimental Model and Subject Details". The data are presented as a ratio of aerobic (O_2) to anaerobic (N_2) cellular Pb^{2+} concentrations and represent the mean ± SD of triplicate cultures. The statistical significance was assessed using a two-sample t-test. These data support **Fig. 6**. n.s. not significant.

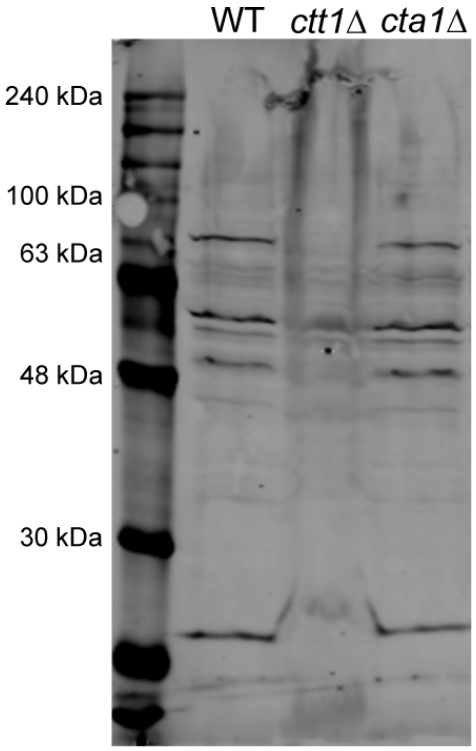

Fig. S5. Validation of the α-Ctt1 antibody. Yeast cytosolic catalase, Ctt1, was probed using a custom antibody generated by Genscript's custom antibody service (Poly Express Premium Service, SC1676). The α-Ctt1 antibody was raised in rabbit against a 1-320 amino acid fragment of Ctt1. The α-Ctt1 antibody was validated in yeast by comparing immunoreactivity between WT, *ctt1*Δ, and *cta1*Δ cells, the latter being a deletion mutant of a peroxisomal/mitochondrial catalase, Cta1, unrelated to Ctt1. All gels were imaged on a LiCOR Odyssey Infrared imager. The expected molecular weight of monomeric Ctt1 is ~64.5 kDa, which is consistent with the highest molecular weight band present in WT and *cta1*Δ cells, but not *ctt1*Δ cells. This antibody was utilized in **Fig. 8B**.

Table S1. List of plasmids.

Name	**Description**	**Source**
p415-*GPD*	pRS415 containing the *GPD* promoter	(2)
p415-*CYC1*	pRS415 containing the *CYC1* promoter	(2)
p316-*GAL1*	pRS316 containing the *GAL1* promoter	(3)
pDH013	HS1 heme sensor subcloned into p415-*GPD*	(4)
pRH021	HS1-M7A heme sensor subcloned into p415-*GPD*	(4)
pJA010	HS1-M7A,H102A heme sensor sub-cloned into p415-*GPD*	(4)
pRH003	eGFP sub-cloned into p415-*GPD*	(4)
pOM003	eGFP sub-cloned into p415-*CYC1*	(4)
pDH039	Cytochrome b_{562} sub-cloned into p316-*GAL1*	This study

Table S2. Mass spectrometry-based protein identification of enolase and GAPDH from the SDS-PAGE gel depicted in **Fig. 7**.

Gel Band	#	Accession	Symbol	% Coverage	# Peptides	PSMs	MW [kDa]	Score Sequest HT
Upper	1	YHR174W	ENO2	65.68	19	381	46.89	1154.83
	2	YGR254W	ENO1	60.87	17	170	46.79	517.04
Lower	1	YGR192C	TDH3	43.67	9	111	35.72	357.34
	2	YJR009C	TDH2	39.76	10	106	35.82	334.19
	3	YJL052W	TDH1	46.99	12	77	35.73	254.91

SUPPLEMENTAL REFERENCES

1. Wissbrock, A., and Imhof, D. (2017) A Tough Nut to Crack: Intracellular Detection and Quantification of Heme in Malaria Parasites by a Genetically Encoded Protein Sensor. *Chembiochem* **18**, 1561-1564
2. Mumberg, D., Muller, R., and Funk, M. (1995) Yeast vectors for the controlled expression of heterologous proteins in different genetic backgrounds. *Gene* **156**, 119-122
3. Kiktev, D. A., Patterson, J. C., Muller, S., Bariar, B., Pan, T., and Chernoff, Y. O. (2012) Regulation of chaperone effects on a yeast prion by cochaperone Sgt2. *Mol Cell Biol* **32**, 4960-4970
4. Hanna, D. A., Harvey, R. M., Martinez-Guzman, O., Yuan, X., Chandrasekharan, B., Raju, G., Outten, F. W., Hamza, I., and Reddi, A. R. (2016) Heme dynamics and trafficking factors revealed by genetically encoded fluorescent heme sensors. *Proc Natl Acad Sci U S A* **113**, 7539-7544